Seismic anisotropy in the lowermost mantle near the Perm Anomaly

Maureen D. Long[1] and Colton Lynner[1]

[1]Department of Geology and Geophysics, Yale University, New Haven, Connecticut, USA

Abstract The lower mantle is dominated by two large structures with anomalously low shear wave velocities, known as Large Low-Shear Velocity Provinces (LLSVPs). Several studies have documented evidence for strong seismic anisotropy at the base of the mantle near the edges of the African LLSVP. Recent work has identified a smaller structure with similar low-shear wave velocities beneath Eurasia, dubbed the Perm Anomaly. Here we probe lowermost mantle anisotropy near the Perm Anomaly using the differential splitting of *SKS* and *SKKS* phases measured at stations in Europe. We find evidence for lowermost mantle anisotropy in the vicinity of the Perm Anomaly, with geographic trends hinting at lateral variations in anisotropy across the boundaries of the Perm Anomaly as well as across a previously unsampled portion of the African LLSVP border. Our observations suggest that deformation is concentrated at the boundaries of both the Perm Anomaly and the African LLSVP.

1. Introduction

The long-wavelength shear wave velocity structure of the lower mantle is dominated by two large regions with anomalously low velocities, known as Large Low-Shear Velocity Provinces (LLSVPs). The Pacific and African LLSVPs represent the most notable structures in lower mantle V_s tomography models [e.g., *Kustowski et al.,* 2008; *Simmons et al.,* 2010; *Dziewonski et al.,* 2010; *Ritsema et al.,* 2011]. Waveform modeling studies using both S waves [e.g., *Ritsema et al.,* 1998; *Ni et al.,* 2002; *Wang and Wen,* 2004] and P waves [*Frost and Rost,* 2014] have suggested that they often have sharp lateral velocity gradients at their edges that typically extend at least ~500 km above the core-mantle boundary (CMB). Normal mode and gravity constraints suggest that the LLSVPs are high-density structures [*Ishii and Tromp,* 1999], and they may correspond to anomalies in both temperature and composition [e.g., *Masters et al.,* 2000; *McNamara and Zhong,* 2005]. The edges of LLSVPs are often associated with structures known as ultralow velocity zones, which correspond to localized but drastic reductions in seismic velocities [*Thorne and Garnero,* 2004; *Rost et al.,* 2010], although this relationship has only been investigated in a few regions.

A variety of models for the origin and evolution of LLSVPs have been proposed, including the idea that they are passive thermochemical piles whose shapes and locations are controlled by mantle convection [e.g., *McNamara and Zhong*, 2005; *Tan et al.,* 2011] and the hypothesis that they represent long-lived structures that have been stable over much of Earth history [e.g., *Dziewonski et al.,* 2010]. Spatial correlations between LLSVPs and large igneous provinces have led to the hypothesis that LLSVP edges represent zones of plume generation [*Burke et al.,* 2008; *Steinberger and Torsvik,* 2012]. Despite recent progress in the geophysical characterization of LLSVPs, however, a number of fundamental questions remain about their origin, evolution, rheology, and dynamics. In particular, it remains unclear how these structures interact with the ambient mantle flow field, and whether mantle convection plays a role in maintaining LLSVPs (or whether LLSVPs play a role in deflecting mantle flow).

A number of recent studies have suggested that the edges of the African LLSVP are associated with strong seismic anisotropy in the lowermost mantle [*Wang and Wen,* 2007; *Cottaar and Romanowicz,* 2013; *Lynner and Long,* 2014a; *Ford et al.,* 2015]. While much of the lower mantle is thought to be (nearly) isotropic [e.g., *Meade et al.,* 1995; *Panning and Romanowicz,* 2006; *Moulik and Ekström,* 2014], there are robust observations of anisotropy in the D″ layer (the lowermost few hundred km of the mantle) in a number of regions [*Nowacki et al.,* 2011, and references therein]. Observations of strong anisotropy at the edges of the African LLSVP suggest the possibility that deformation is concentrated at LLSVP boundaries, perhaps due to a contrast in rheology or to specific geodynamic processes such as focused upwelling. While observations of anisotropy at LLSVP edges are robust, their interpretation in terms of mantle flow remains challenging due to limitations

in our knowledge of the elasticity and deformation of relevant materials at D″ conditions and a general paucity of measurements over a range of orientations [*Ford et al.,* 2015].

Lekic et al. [2012] recently applied cluster analysis to a suite of lower mantle shear velocity tomography models and identified a mesoscale structure with smaller dimensions than the African and Pacific LLSVPs but a similar reduction in seismic velocity located roughly beneath the city of Perm, Russia. This structure, dubbed the "Perm Anomaly," has a diameter of roughly 1000 km, representing roughly 5% of the area of either LLSVP. Tomographic imaging and waveform modeling suggest strong lateral gradients in isotropic shear velocity at the edges of this structure [*Lekic et al.,* 2012], although the sharpness and precise location of its sides remain to be elucidated in full. *Lekic et al.* [2012] suggest that the Perm Anomaly may represent compositionally distinct material that is similar to the material that makes up the LLSVPs. It is unclear, however, how the Perm Anomaly interacts dynamically with the rest of the mantle, and whether the processes that led to the formation of the Perm Anomaly are similar to those that formed the substantially larger LLSVP structures.

Here we investigate seismic anisotropy in the lowermost mantle in the vicinity of the Perm Anomaly and compare its anisotropic character to that of the nearby African LLSVP. The work presented here builds on a previous study by *Lynner and Long* [2014a], who applied differential *SKS-SKKS* shear wave splitting analysis to characterize anisotropy in the vicinity of the African LLSVP. We present measurements of *SKS-SKKS* splitting discrepancies measured at 18 permanent stations in Europe. These phases sample the lowermost mantle around the Perm Anomaly, as well as a northern portion of the African LLSVP border. We find evidence for strong variations in anisotropy associated with the Perm Anomaly structure, as well as along the African LLSVP border.

2. Data and Methods

The measurement and interpretation of *SKS-SKKS* splitting discrepancies rely on the fact that *SKS* and *SKKS* have very similar paths in the upper mantle but sample different volumes of the lowermost mantle. Pronounced differences in splitting behavior between the two phases (measured for the same event-station pair) imply a contribution from lowermost mantle anisotropy to one or both phases [e.g., *Niu and Perez,* 2004]. This is often interpreted as lateral variability in anisotropic strength and/or geometry [e.g., *Niu and Perez,* 2004; *Long,* 2009]. Alternatively, it may reflect the presence of lowermost mantle anisotropy in a geometry that splits *SKS* and *SKKS* phases differently. A discussion of the assumptions and limitations of the *SKS-SKKS* splitting discrepancy technique is contained in the supporting information.

We follow the same data processing and measurement procedure as in our previous work on *SKS-SKKS* splitting discrepancies [*Long,* 2009; *Lynner and Long,* 2014a]. We selected 18 seismic stations located in Europe for our analysis (Figure 1), beneath which the upper mantle anisotropy is well characterized [*Lynner and Long,* 2013, 2014b; *Ford et al.,* 2015]. We have restricted our analysis to stations that exhibit either (1) relatively consistent *SKS* splitting parameters over a range of back azimuths, indicating generally simple upper mantle anisotropy, or (2) consistent null (that is, nonsplit) *SKS* arrivals over a wide back azimuthal swath, indicating an apparently isotropic upper mantle. These criteria allow us to correct for the effect of upper mantle anisotropy beneath the station, as described in section 4. Station information and upper mantle corrections are shown in the supporting information Table S1, and supporting information Figure S1 shows examples of *SKS* splitting patterns for representative stations. Anisotropy in the lowermost mantle does not make the primary contribution to *SK(K)S* splitting at any of the stations examined in this study, but the *SKS-SKKS* discrepancy technique allows us to identify the small minority of phases that are affected by D″ anisotropy.

We selected earthquakes of magnitude 5.8 or greater in the epicentral distance range from $\Delta = 108°$ to $122°$ for analysis and identified records with clear *SKS* and *SKKS* arrivals on the same seismogram. The SplitLab software [*Wüstefeld et al.,* 2008] was used to preprocess the data and measure shear wave splitting parameters (fast direction, ϕ, and delay time, δt) for each phase. Each record was bandpass filtered between 0.04 and 0.125 Hz (the same filter used in the previous *SKS* analysis of upper mantle anisotropy); in a small minority of cases, we adjusted the corner frequencies slightly to optimize signal-to-noise ratio. We applied the transverse component minimization and the rotation-correlation measurement methods simultaneously and only retained measurements for which both methods agreed within the 95% confidence regions. We allowed for average errors of up to ±30° in ϕ and ±1.2 s in δt (95% confidence regions), but most measurements have
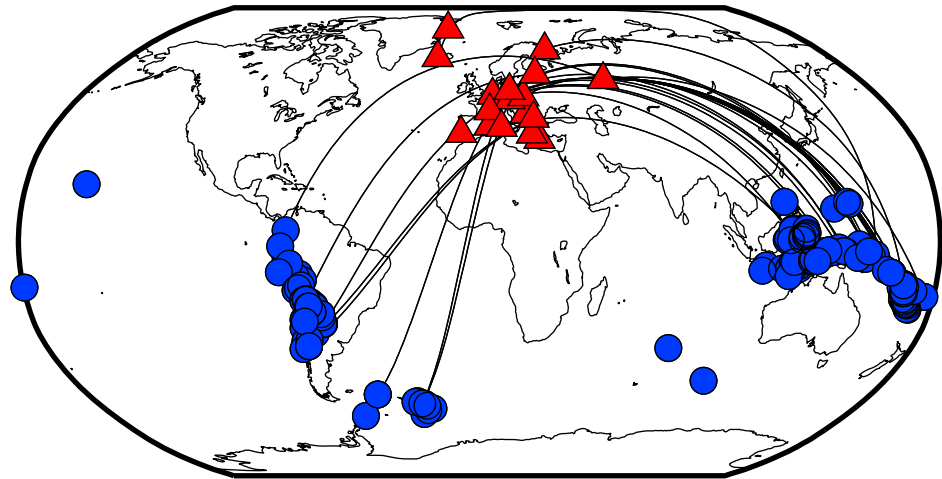
Figure 1. Map of stations (red triangles) and events (blue circles) used in this study. Black lines represent great circle paths for the 30 event-station pairs that exhibited *SKS-SKKS* splitting discrepancies.

errors of less than ±15° and ±0.8 s, respectively. We classified as null those arrivals with a clear phase arrival, high signal-to-noise ratio, and (nearly) linear particle motion.

We characterized as discrepant those *SKS-SKKS* pairs for which one phase was null and the other was clearly split, with a 95% confidence region on delay time that did not encompass zero, or (in one case) when both phases were split but the 95% confidence regions did not overlap. Pairs for which both phases were null, or both phases were split with similar splitting parameters, were characterized as nondiscrepant. Waveform and particle motion diagram examples for three discrepant *SKS-SKKS* pairs are shown in Figure 2.

3. Results and Geographic Trends

Our analysis yielded 180 well-constrained *SKS-SKKS* pairs at 18 stations, with 30 of those pairs exhibiting clear splitting discrepancies (supporting information Table S2). At least one *SKS-SKKS* pair was identified at every station, and 10 of the 18 stations exhibited at least one discrepant pair. Stations ARU, BORG, GRA1, LVZ, and VSU made the largest contributions to the data set, while stations ARU, GRA1, RUE, and VTS each contributed more than one discrepant pair. For 12 of the 30 discrepant pairs, the *SKS* phase is split while the corresponding *SKKS* is null; for the remaining 17, the *SKKS* arrival is split while the corresponding *SKS* is null. In one case, we measured a pair for which both phases were split, with measured fast directions that differed by about 80°. For the vast majority (~90%) of the 150 nondiscrepant pairs, both phases were null. We did not observe any systematic difference in the prevalence of discrepant *SKS-SKKS* measurements for stations with "simple" versus "null" upper mantle anisotropy patterns. Of the 10 stations that exhibited discrepancies, 7 were simple and 3 were null, while of the 8 stations that did not, 4 were simple and 4 were null.

Figure 3 shows our results in map view on top of the GyPSuM *S* wave velocity model [*Simmons et al.,* 2010] and the cluster analysis of *Lekic et al.* [2012], which highlights regions where different tomographic models agree that there are anomalously low *S* wave speeds. We used TauP [*Crotwell et al.,* 1999] to calculate pierce points using the iasp91 one-dimensional Earth velocity model at a depth of 2700 km in the mantle. Discrepant pairs highlight regions where a difference in splitting argues for a contribution from seismic anisotropy in the lowermost mantle. Nondiscrepant pairs highlight paths over which there is no evidence for a contribution to splitting from lowermost mantle anisotropy, although such a contribution cannot be entirely ruled out.

It is clear from Figure 3 that the nondiscrepant and discrepant pairs are not randomly distributed throughout the study region. Rather, the discrepant *SKS-SKKS* pairs in our data set preferentially sample three regions, although they are often interspersed with nondiscrepant pairs. First, there is a group of discrepant pairs that sample the edge of the African LLSVP beneath northern Africa, the Iberian Peninsula, and the United Kingdom. These measurements are consistent with previous work suggesting a contrast in anisotropy across the African LLSVP boundary [*Wang and Wen,* 2007; *Cottaar and Romanowicz,* 2013; *Lynner and Long,* 2014a] and extend this observation to a previously unsampled northern portion of the LLSVP border. Second,
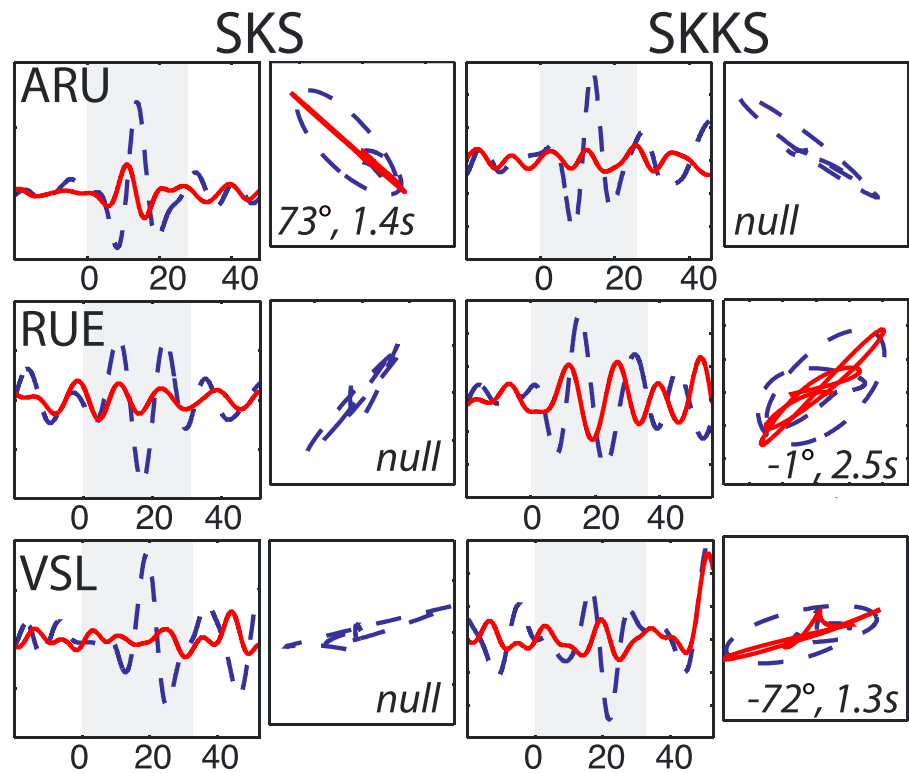
Figure 2. Waveform examples for three discrepant *SKS-SKKS* pairs that sample the Perm Anomaly, measured at three different stations (station names at left). (first column) The radial (dashed blue line) and transverse (solid red line) component of the *SKS* phase, with the time window used in the measurement shown in gray. (second column) A particle motion diagram for the *SKS* phase (dashed blue line), with the particle motion after correction for splitting shown with a solid red line (for nonnull measurements only). Measured splitting parameters are shown at the bottom of the particle motion diagram. (third and fourth columns) The corresponding *SKKS* phases.
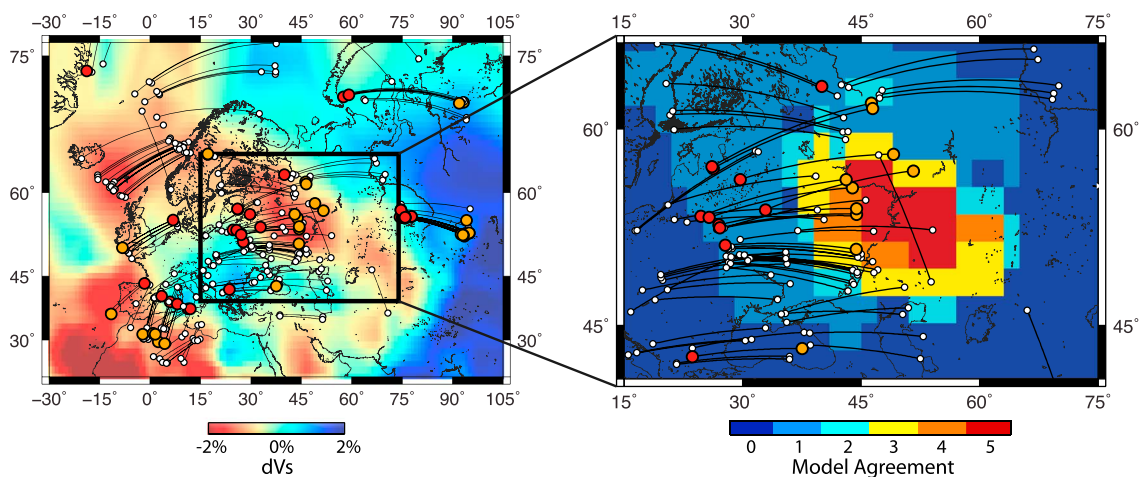

Figure 3. (left) Discrepant and nondiscrepant pairs plotted on top of the GyPSuM tomography model at a depth of 2700 km. Nondiscrepant pairs (including both null-null pairs and split-split pairs) are shown with white dots, with lines connecting the *SKS* and *SKKS* pierce points at 2700 km. Discrepant pairs are shown with colored dots for *SKS* (red) and *SKKS* (orange). (right) Same measurements plotted on top of the cluster analysis of *Lekic et al.* [2012], zoomed in to the Perm Anomaly region. Background colors indicate the number of tomography models that agree that a given region is anomalously slow.

we observe a group of 10 discrepant pairs that appear to sample near the edges of the Perm Anomaly, as delineated by cluster analysis (Figure 3). These discrepant pairs sample over a roughly 60° azimuthal range of propagation directions, measured at four different stations, making it unlikely that this observation is an artifact due to unusual structure beneath a single station. Third, there is a group of discrepant measurements that sample directly to the north and south of (60°N, 80°E), just to the east of the Perm Anomaly (Figure 3, right). This region is associated with a pronounced lateral gradient in isotropic wave speeds in the GyPSuM tomography model (Figure 3, left).

4. Correction for Upper Mantle Anisotropy

The maps in Figure 3 provide evidence for lowermost mantle anisotropy sampled by the discrepant *SKS* and *SKKS* pairs. In order to directly constrain splitting from the lowermost mantle, we must explicitly correct for the effect of upper mantle anisotropy. We carried out such a correction in a way that aims to minimize bias in our estimates of lowermost mantle splitting. We treat discrepant pairs and nondiscrepant pairs differently to avoid introducing spurious signal into the nondiscrepant pairs. For nondiscrepant pairs, we focused our interpretation on the 90% of pairs that involve a null arrival for both *SKS* and *SKKS*. The interpretation of this subset of measurements is most straightforward under two circumstances: (1) when the station overlies apparently isotropic upper mantle or (2) when the initial polarization of the *SK(K)S* phases aligns near (within ±20°) a fast or slow direction of upper mantle anisotropy. In either of these cases, the waveforms are not affected by anisotropy in the upper mantle, so we can interpret the lack of *SK(K)S* splitting as reflecting a lack of contribution from lowermost mantle anisotropy. From the set of 136 null-null pairs, we identified a subset of 61 that met the above criteria, for which we can rule out a contribution from anisotropy in the lowermost mantle.

For discrepant *SKS-SKKS* pairs, on the other hand, there is clear evidence for a contribution from lowermost mantle anisotropy to the splitting of one or both phases, and an explicit correction for upper mantle anisotropy to isolate the lowermost mantle signal is appropriate. For each of these pairs, we used the average SKS splitting parameters (see corrections in Table S1), which we take to be a first-order estimate of the upper mantle contribution, and rotated and time shifted the horizontal component seismograms to account for splitting due to upper mantle anisotropy. We then remeasured the splitting of the corrected *SKS* and *SKKS* phases using our original measurement procedures. Not all of the waveforms yielded a well-constrained measurement after the upper mantle correction, but of the 60 corrected phases, we obtained 10 splitting measurements and 17 null arrivals that directly constrain the D″ contribution.

All 149 measurements of lowermost mantle splitting (139 nulls + 10 splits) are shown in Figure 4 and supporting information Table S3. Null measurements dominate the regions away from the LLSVP edge and the Perm Anomaly. We observe well-resolved splitting in the vicinity of the Perm Anomaly, with one group of fast directions oriented nearly N-S and one group oriented nearly E-W. There is one split measurement that appears to sample the interior of the anomaly, while the others appear to sample its edges (Figure 4). Along the African LLSVP edge, the split measurements appear to sample the LLSVP border (or just inside it) and are interspersed with null measurements. We also resolve splitting due to lowermost mantle anisotropy in the easternmost part of our study region, to the east of the Perm Anomaly.

5. Discussion

As in any study of lowermost mantle anisotropy, it is important to rule out possible effects that could be misinterpreted as splitting due to D″ anisotropy. We can rule out scattering from isotropic structure as a primary cause of transverse component energy, as we only retained splitting measurements for which the pulse shape of the transverse component was similar to the time derivative of the radial component [e.g., *Lynner and Long,* 2014a]. While finite frequency effects can cause small differences estimates of splitting parameters between *SKS* and *SKKS* phases [*Lin et al.,* 2014], large discrepancies such as those documented here require a contribution from the lower mantle. Finally, given that we document similar geographic patterns of lowermost mantle anisotropy over a range of stations in this study, we can rule out shallow anisotropic heterogeneity in the crust or uppermost mantle lithosphere as a primary explanation for the discrepancies.

We also investigated whether interference from other phases or changes in *SK(K)S* polarizations may have affected the measurements. Supporting information Figure S2 shows a histogram of the number of discrepant and non-discrepant pairs as a function of epicentral distance. This diagram shows that the discrepant measurements are
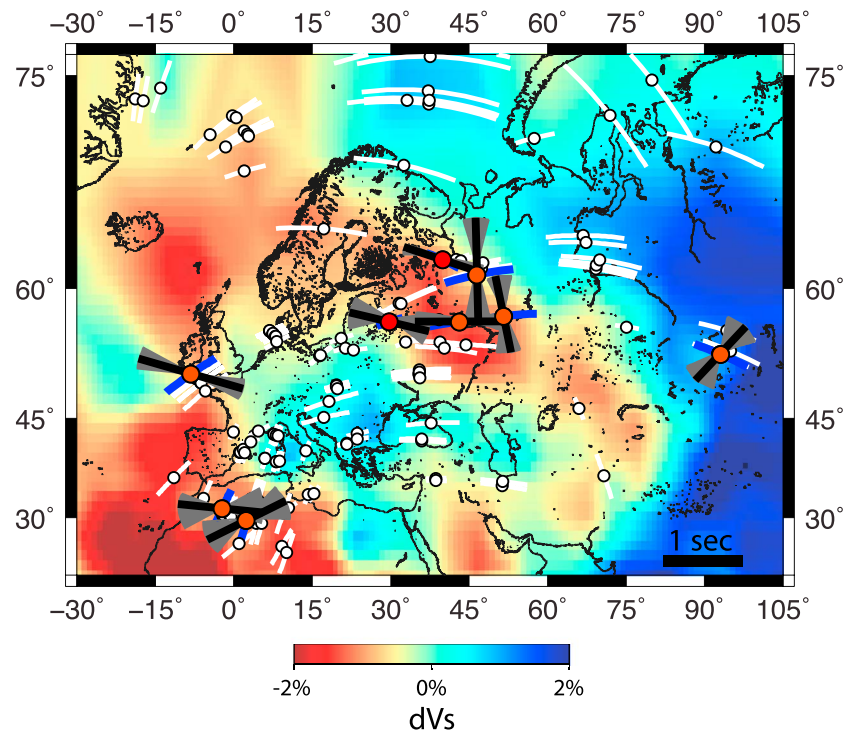
Figure 4. Map of lowermost mantle splitting with contributions from the upper mantle removed. Background colors indicate shear velocities, as in Figure 3. White dots indicate null observations, where splitting due to lowermost mantle anisotropy can be ruled out, while the white lines indicate the portion of the *SK(K)S* paths through the D″ layer for null measurements. Measurements of lowermost mantle splitting are plotted as bars oriented in the fast direction (as measured at the station) and scaled by delay time. Blue lines indicate the portion of the *SK(K)S* paths through the D″ layer for nonnull measurements. Gray shaded regions indicate the 95% confidence region on the fast direction estimates. Red dots indicate split *SKS* phases, orange dots indicate split *SKKS* phases.

distributed fairly evenly over the epicentral distance range, and that the type of discrepancy (that is, *SKS* null and *SKKS* split, or vice versa) also does not depend on distance. Furthermore, we do not observe any systematic trends in the observed delay times for D″-associated splitting as a function of distance (supporting information Figure S3). We can thus rule out interference from other phases as the primary cause for the observed discrepancies. *Restivo and Helffrich* [2006] suggested that modifications of *SK(K)S* polarizations due to CMB topography or other dipping structures at the base of the mantle may cause discrepant splitting. This is unlikely to be the primary contribution to our data set, as it would cause noticeable polarization anomalies in both the uncorrected and corrected particle motion diagrams, which we did not observe (supporting information). Therefore, we interpret our measurements as likely reflecting lateral variations in seismic anisotropy (strength and/or geometry) at the base of the mantle. An alternative explanation is a style of anisotropy in the lowermost mantle that leads to discrepant splitting between *SKS* and *SKKS* because of their different propagation directions. In either case, our discrepant observations require a contribution from lowermost mantle anisotropy to one or both phases.

The geographic pattern of *SKS-SKKS* splitting discrepancies documented in this study suggests that seismic anisotropy—and thus deformation—is concentrated in the lowermost mantle near regions where there are strong lateral gradients in shear velocity. To visualize these relationships more clearly, we have plotted our results as a function of distance from the center of the Perm Anomaly or the edge of the African LLSVP (supporting information Figure S4) and on a map of lateral *Vs* gradients (supporting information Figure S5) that show the edges of the African LLSVP and Perm Anomaly [*Lekic et al.,* 2012]. In map view, it is apparent that the easternmost group of discrepant splits in our study (near 60°N, 80°E) lies just to the east of the ring of sharp *Vs* gradients that surround the Perm Anomaly. Given this geographical overlap, it is possible that this group of discrepant measurements is associated with the Perm Anomaly structure. An alternative interpretation is that it is associated with the edge of a major fast anomaly beneath Eurasia visible in the GyPSuM tomography model (Figure 3) and other models.

We have documented lowermost mantle anisotropy that (qualitatively) ==coincides geographically with the inferred edges of both the African LLSVP and the much smaller Perm Anomaly.== While the origin and evolution of these structures remain to be fully elucidated, our observations suggest that they may interact with mantle flow in a similar way. There are several possible scenarios that may result in strong deformation concentrated at the edge of low-shear velocity provinces (LSVPs) such as the African and Pacific LLSVPs and the Perm Anomaly. One possibility is that LSVP material has a higher viscosity than the ambient mantle and is thus resistant to deformation, leading to relatively strong anisotropy at LSVP edges as ambient mantle flow is deflected. However, this scenario contrasts with the interpretation of low V_s in terms of a positive thermal anomaly, which would imply a lower viscosity (at least for an isochemical mantle). Another possibility is that the anisotropy reflects local geodynamic processes, such as focused upwelling [e.g., *Steinberger and Torsvik*, 2012]. In any case, the observation of seismic anisotropy at the edges of both the African LLSVP and the Perm Anomaly may be used to constrain models for their formation and evolution.

6. Summary

We have presented *SKS-SKKS* splitting measurements that reveal evidence for lateral variability in lowermost mantle anisotropy beneath Eurasia. Our data set allows for a straightforward comparison between the African LLSVP edge and the Perm Anomaly using phases measured at the same stations. We find evidence for ==anisotropy near the borders of both the African LLSVP and the Perm Anomaly, implying that deformation is concentrated at the edges of both structures. This suggests in turn that the Perm Anomaly may interact with ambient mantle flow in a manner similar to the African LLSVP, despite the difference in size,== and is consistent with the hypothesis that it is made of the same type of material as the LLSVPs. Models for the origin, evolution, and dynamics of LSVPs must be consistent with the observation of strong anisotropy in the lowermost mantle at their edges. Measurements such as those presented here could potentially be used to explicitly test predictions of geodynamical models for the formation and evolution of LLSVPs and mesoscale low-velocity structures.

References

Burke, K., B. Steinberger, T. H. Torsvik, and M. A. Smethurst (2008), Plume generation zones at the margins of Large Low Shear Velocity Provinces on the core-mantle boundary, *Earth Planet. Sci. Lett.*, *265*, 49–60.

Cottaar, S., and B. Romanowicz (2013), Observations of changing anisotropy across the southern margin of the African LLSVP, *Geophys. J. Int.*, *195*(2), 1184–1195.

Crotwell, H. P., T. J. Owens, and J. Ritsema (1999), The TauP Toolkit: Flexible seismic travel-time and ray-path utilities, *Seismol. Res. Lett.*, *70*, 154–160.

Dziewonski, A. M., V. Lekic, and B. Romanowicz (2010), Mantle anchor structure: An argument for bottom up tectonics, *Earth Planet. Sci. Lett.*, *299*, 69–79.

Ford, H. A., M. D. Long, X. He, and C. Lynner (2015), Lowermost mantle flow at the eastern edge of the African Large Low Shear Velocity Province, *Earth Planet. Sci. Lett.*, *420*, 12–22.

Frost, D. A., and S. Rost (2014), The P-wave boundary of the Large-Low Shear Velocity Province beneath the Pacific, *Sci. Lett.*, *403*, 380–392.

Ishii, M., and J. Tromp (1999), Normal-mode and free-air gravity constraints on lateral variations in velocity and density of the Earth's mantle, *Science*, *285*, 1231–1236.

Kustowski, B., G. Ekström, and A. M. Dziewonski (2008), Anisotropic shear-wave velocity structure of the Earth's mantle: A global model, *J. Geophys. Res.*, *113*, B06306, doi:10.1029/2007JB005169.

Lekic, V., S. Cottaar, A. M. Dziewonski, and B. Romanowicz (2012), Cluster analysis of global lower mantle tomography: A new class of structure and implications for chemical heterogeneity, *Earth Planet. Sci. Lett.*, *357–358*, 68–77.

Lin, Y.-P., L. Zhao, and S.-H. Hung (2014), Full-wave effects on shear wave splitting, *Geophys. Res. Lett.*, *41*, 799–804, doi:10.1002/2013GL058743.

Long, M. D. (2009), Complex anisotropy in D″ beneath the eastern Pacific from SKS-SKKS splitting discrepancies, *Earth Planet. Sci. Lett.*, *285*, 181–189.

Lynner, C., and M. D. Long (2013), Sub-slab seismic anisotropy and mantle flow beneath the Caribbean and Scotia subduction zones: Effects of slab morphology and kinematics, *Earth Planet. Sci. Lett.*, *361*, 367–378.

Lynner, C., and M. D. Long (2014a), Lowermost mantle anisotropy and deformation along the boundary of the African LLSVP, *Geophys. Res. Lett.*, *41*, 3447–3454, doi:10.1002/2014GL059875.

Lynner, C., and M. D. Long (2014b), Sub-slab anisotropy beneath the Sumatra and circum-Pacific subduction zones from source-side shear wave splitting observations, *Geochem. Geophys. Geosyst.*, *15*, 2262–2281, doi:10.1002/2014GC005239.

Masters, G., G. Laske, H. Bolton, and A. Dziewonski (2000), The relative behavior of shear velocity, bulk sound speed, and compressional velocity in the mantle: Implications for chemical and thermal structure, in *Earth's Deep Interior: Mineral Physics and Tomography From the Atomic to the Global Scale*, AGU Monogr. Ser., vol. 117, edited by S. Karato et al., pp. 63–87, AGU, Washington, D. C.

McNamara, A. K., and S. Zhong (2005), Thermochemical structures beneath Africa and the Pacific Ocean, *Nature*, *437*, 1136–1139, doi:10.1038/nature04066.

Meade, C., P. G. Silver, and S. Kaneshima (1995), Laboratory and seismological observations of lower mantle isotropy, *Geophys. Res. Lett.*, *22*, 1293–1296, doi:10.1029/95GL01091.

Moulik, P., and G. Ekström (2014), An anisotropic shear velocity model of the Earth's mantle using normal modes, body waves, surface waves, and long-period waveforms, *Geophys. J. Int.*, *199*, 1713–1738.

Ni, S., E. Tan, M. Gurnis, and D. Helmberger (2002), Sharp sides to the African superplume, *Science*, *296*, 1850–1852.

Niu, F., and A. M. Perez (2004), Seismic anisotropy in the lower mantle: A comparison of waveform splitting of SKS and SKKS, *Geophys. Res. Lett.*, *31*, L24612, doi:10.1029/2004GL0211196.

Nowacki, A., J. Wookey, and J. M. Kendall (2011), New advances in using seismic anisotropy, mineral physics and geodynamics to understand deformation in the lowermost mantle, *J. Geodyn.*, *52*, 205–228.

Panning, M., and B. Romanowicz (2006), A three-dimensional radially anisotropic model of shear velocity in the whole mantle, *Geophys. J. Int.*, *167*, 361–379.

Restivo, A., and G. Helffrich (2006), Core-mantle boundary structure investigated using *SKS* and *SKKS* polarization anomalies, *Geophys. J. Int.*, *165*, 288–302.

Ritsema, J., S. Ni, D. V. Helmberger, and H. P. Crotwell (1998), Evidence for strong shear velocity reductions and velocity gradients in the lower mantle beneath Africa, *Geophys. Res. Lett.*, *25*, 4245–4248, doi:10.1029/1998GL900127.

Ritsema, J., A. Deuss, H. J. van Heijst, and J. H. Woodhouse (2011), S40RTS: A degree-40 shear-velocity model for the mantle from new Rayleigh wave dispersion, teleseismic traveltime and normal-mode splitting function measurements, *Geophys. J. Int.*, *184*, 1223–1236.

Rost, S., E. J. Garnero, and W. Stefan (2010), Thin and intermittent ultralow-velocity zones, *J. Geophys. Res.*, *115*, B06312, doi:10.1029/2009JB006981.

Simmons, N. A., A. Forte, L. Boschi, and S. Grand (2010), GyPSuM: A joint tomographic model of mantle density and seismic wave speeds, *J. Geophys. Res.*, *115*, B12310, doi:10.1029/2010JB007631.

Steinberger, B., and T. H. Torsvik (2012), A geodynamic model of plumes from the margins of Large Low Shear Velocity Provinces, *Geochem. Geophys. Geosyst.*, *13*, Q01W09, doi:10.1029/2011GC003808.

Tan, E., W. Leng, S. Zhong, and M. Gurnis (2011), On the location of plumes and lateral movement of thermochemical structures with high bulk modulus in the 3-D compressible mantle, *Geochem. Geophys. Geosyst.*, *12*, Q07005, doi:10.1029/2011GC003665.

Thorne, M. S., and E. J. Garnero (2004), Inferences on ultralow-velocity zone structure from a global analysis of SPdKS waves, *J. Geophys. Res.*, *109*, B08301, doi:10.1029/2004JB003010.

Wang, Y., and L. Wen (2004), Mapping the geometry and geographic distribution of a very low velocity province at the base of the Earth's mantle, *J. Geophys. Res.*, *109,* B10305, doi:10.1029/2003JB002674.

Wang, Y., and L. Wen (2007), Complex seismic anisotropy at the border of a very low velocity province at the base of the Earth's mantle, *J. Geophys. Res.*, *112*, B09305, doi:10.1029/2006JB004719.

Wessel, P., and W. H. F. Smith (1999), Free software helps map and display data, *Eos Trans AGU*, *72*, 441, doi:10.1029/90EO00319.

Wüstefeld, A., G. Bokelmann, G. Barruol, and C. Zaroli (2008), Splitlab: A shear-wave splitting environment in Matlab, *C. R. Geosci.*, *34*, 515–528.